

Nitrogen-doped graphene loaded non-noble Co catalysts for liquid-phase cyclohexane oxidation with molecular oxygen

Fang Hao, Yuan Sun, Yidi Wang, Yang Lv, Pingle Liu[†], Wei Xiong[†], and Hean Luo

College of Chemical Engineering, National & Local United Engineering Research Centre for Chemical Process Simulation and Intensification, Xiangtan University, Xiangtan 411105, China

(Received 17 February 2021 • Revised 26 April 2021 • Accepted 26 April 2021)

Abstract—Selective aerobic oxidation of cyclohexane to cyclohexanone and cyclohexanol (KA oil) with high yield under mild and green conditions is still a significant challenge in the current chemical industry. Herein, nitrogen doped graphene loaded non-noble Co (Co-N-rGO) catalysts, prepared by a facile post-impregnation method, exhibited a high catalytic performance and stability in liquid phase cyclohexane oxidation with molecular oxygen. The experiment and characterization results show that N doping in the catalysts promotes Co metal particle dispersion and induces carbon film coating on Co to prevent leaching and agglomeration. Besides, density functional theory (DFT) calculations show that N doping is beneficial to the O-O bonds breaking in cyclohexyl-hydroperoxides (CHHP), thereby promoting the dissociation of CHHP and enhancing the yield to KA oil. In addition, the catalyst can be easily separated without appreciable loss of catalytic activity after recycling for five times, and show potential industrial application value for the catalytic oxidation of cyclohexane to KA oil in the chemical industry.

Keywords: N-doped Graphene, Non-noble Co Catalysts, Selective Oxidation, Cyclohexane, KA Oil

INTRODUCTION

Catalytic oxidation of cyclohexane to obtain cyclohexanone-cyclohexanol mixtures (KA oil) is a crucial reaction since KA oil is key precursor in the synthesis of polymers nylon-6, nylon-66, and adipic acid [1]. The current industrial processes for selective oxidation of cyclohexane utilize homogeneous cobalt or manganese salts as catalysts at 125-165 °C and oxygen pressure of 0.8-1.5 MPa. However, it is a low efficient reaction since that cyclohexane conversion is often kept below 5% for obtaining high yield to KA oil by inhibiting its deep oxidation [2,3]. Besides, the recovery of homogeneous catalyst from the liquid phase is usually costly and causes many environmental problems. To overcome these drawbacks, developing highly efficient and environmentally friendly heterogeneous catalysts has been highly desirable.

To date, many new heterogeneous catalysts for the aerobic oxidation of cyclohexane have been developed, including metal oxides [4-7], molecular sieves supported metals [8,9], metal organic complex (such as metalloporphyrin [10] and Schiff based compounds [11]), metal organic framework (MOFs) catalysts [12,13], bimetallic supported catalysts [12,13], and any other new materials [14]. Among them, Zhang et al. developed Co-based spinel nanocrystal catalysts and obtained 17.2% cyclohexane conversion with 95.3% selectivity to KA oil under O₂ pressure of 2.0 MPa [12]. Wu et al. prepared bimetallic Au-Pt and Au-Pd supported on mesoporous silica, and obtained cyclohexane conversion of 6.4% with 99.5% selectivity to KA-oil [15]. Xu et al. prepared a porous honeycomb-like nano-

structure with N doping supported bimetallic Ce-Cr oxide and achieved 56.5% conversion of cyclohexane with 95.5% selectivity to KA oil by using tert-Butyl hydroperoxide (TBHP) as oxidant and acetonitrile as the solvent [16]. Ye et al. found that cyclohexane conversion of 13.6% and 92% selectivity to KA oil could be achieved by the porous material PMS-1 by using acetonitrile as the solvent [14]. Although new heterogeneous catalysts exhibit excellent performance in the cyclohexane oxidation, severe reaction conditions, high cost of noble metals and oxidants, and environmentally unfriendly addition of solvents significantly limit their further applications. Therefore, it is still highly desirable to design a recyclable catalyst that is cheap, solvent-free, easy-to-handle, and highly efficient for the aerobic oxidation of cyclohexane.

Graphene prepared from graphite has been widely applied in many fields for its high electron mobility, high surface area, and high thermostability. It has been reported that the defects in carbonaceous framework can be considered as effective active sites for catalysis [17-19]. Thus, defective graphene has been widely studied and used in oxidation reactions [20-24]. Besides, graphene can be also applied as support to load active metals in many catalysis fields. However, active metal nanoparticles tend to aggregate due to the low binding energy of metal nanoparticles (NPs) anchored on the original graphene surface [25]. Hence, researchers developed various strategies to stabilize metal NPs on graphene, and substitutional doping the graphene matrix with heteroatoms (mainly nitrogen and boron) represents a convenient route [26]. The aggregation of metal NPs is greatly restricted because of the enhanced metal-support interaction by the strong bonding between N doping sites and metal NPs [27-29]. For instance, Ni@NG (N-doped graphene), Cu/NG, and Pd/N-HOPG (highly oriented pyrolytic graphite) show good dispersion of metal NPs, as well as greatly enhanced catalytic

[†]To whom correspondence should be addressed.
E-mail: liupingle@xtu.edu.cn, happy.xiongw@163.com
Copyright by The Korean Institute of Chemical Engineers.

activity and stability in methanation [30], methanol oxidation [31], and oxygen-reduction reaction [32].

In this work, a series of N-doped graphene loaded Co (Co-N-rGO) catalysts were prepared *via* a facile post-impregnation synthesis method. The physical and chemical properties of catalysts were systematically analyzed. And the catalytic activity was evaluated in liquid phase catalytic oxidation of cyclohexane with oxygen as an oxidant. These Co-N-rGO catalysts show good catalytic performance and stability without solvent addition. The influence of O₂ pressure, reaction temperature and reaction time on the reaction was also investigated. DFT calculations were carried out to verify the role of nitrogen doping in the dissociation of CHHP. This work will provide a rational strategy for development of highly active and stable non-noble metal catalysts for oxidation of cyclohexane.

EXPERIMENTAL

1. Materials

Cyclohexane (99.7%), sodium nitrate (99.0%), concentrated hydrochloric acid (36-38%), hydrogen peroxide (30%) and potassium permanganate (99.5%) were purchased from Tianjin Kemiou Chemical Reagent Co., Ltd. Chlorobenzene (99.0%), triphenylphosphine (99.0%) and melamine (99.0%) were purchased from Sinopharm Chemical Reagent Co., Ltd. Concentrated sulfuric acid (95-98%) and absolute ethanol (99.7%) were purchased from Hunan Huihong Reagent Co., Ltd.

2. Preparation of Catalysts

Graphene oxide (GO) was synthesized through a modified Hummers' method [33]. In a typical procedure, we added sodium nitrate (0.5 g) and graphite (0.5 g) to concentrated sulfuric acid (22 mL) and stirred for 8 min in ice bath. 3 g of potassium permanganate was slowly added with constant stirring for 30 min. Then, the mixture was placed in a water bath and continuously stirred for another 1 h at 45 °C. Subsequently, 45 mL of deionized water was slowly added to the mixture, and the suspension obtained from the mixture was transferred into an oil bath and continuously stirred for 1 h at 95 °C. Then, the suspension was treated with 30% hydrogen peroxide. The suspension was centrifuged and washed several times by 5% hydrochloric acid and distilled water. Finally, the sample was dried by lyophilization, and the GO was obtained. The physical morphology of GO is shown in Fig. 1.

For the preparation of Co-N-rGO, melamine (0.18 g) and cobalt

acetate (0.4 g) were first dissolved in water and ethanol mixture (30 ml), respectively. After the two solutions were mixed via ultrasonication for 20 min at room temperature, the former obtained GO (0.4 g) was added to it. The mixture was heated to 80 °C in an oil bath to remove water under stirring, dried at 80 °C overnight. After that, the solid was ground finely and calcined under nitrogen at the specific temperature for 2 h with a ramping rate of 2 °C·min⁻¹. The obtained catalysts were denoted as Co-N-rGO-T (T represents the calcination temperature, T=600, 700, 800 and 900 °C).

For comparison, Co-N-800, Co-rGO-800, N-rGO-800 were also prepared with the same procedure, except that GO, melamine or cobalt acetate were not added, respectively, during their synthesis procedures. The three samples were calcined under nitrogen for 2 h at 800 °C.

For comparison of the synthesis method, Co/NrGO and Co/NrGO were prepared. Co/NrGO was prepared by a hydrothermal process [34]. 0.18 g of melamine and 0.4 g of cobalt acetate were dissolved in 30 ml water and ethanol mixed solution, respectively. After the two solutions were mixed and ultrasonicated for 20 minutes at room temperature, the previous obtained GO (0.4 g) was added, and the mixture was transferred into a Teflon-lined stainless steel autoclave (at 160 °C for 12 h). Then, the solid was centrifuged and dried overnight at 80 °C after cooling to room temperature, and finally calcined in nitrogen at 800 °C for 2 h. The catalyst was denoted as Co/NrGO. The difference between Co/NrGO and Co/NrGO preparation was the introduction time of cobalt acetate precursor. For Co/NrGO synthesis [34], cobalt acetate solution was added after the hydrothermal procedure of melamine and GO mixture. The other conditions were kept the same, and the obtained catalyst was Co/NrGO. Both samples were calcined under nitrogen for 2 h at the same temperature of 800 °C.

3. Catalyst Characterization

X-ray diffraction (XRD) measurements were operated at 40 mA and 30 kV on a Japan Rigaku D/Max 2550VB+ 18 kW diffractometer (Cu K α radiation) in the range of 5 to 90° at a scanning rate of 2°·min⁻¹. A field emission SEM (Zeiss Gemini 300) was used to characterize the specific morphology. Transmission electron microscopy (TEM) was measured on an FEI Tecnai F20 ST microscope at 200 kV to observe the morphology and detailed microstructure. N₂ adsorption-desorption isotherms were obtained from a Micromeritics ASAP 2020 analyzer at 77 K. The pore size distribution was calculated by using the Barret-Joyner-Halenda (BJH)

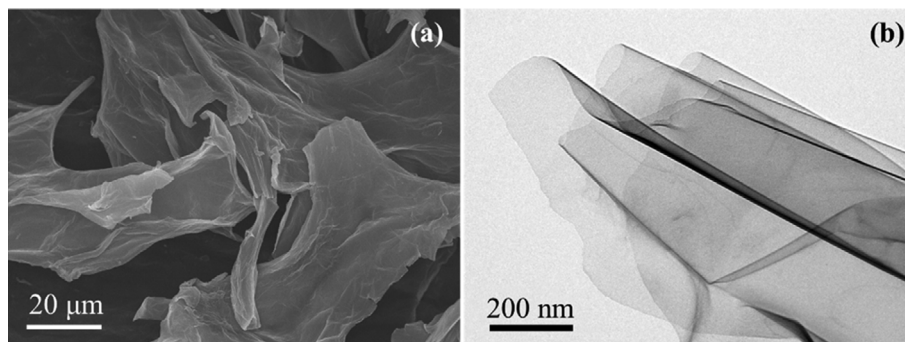


Fig. 1. SEM (a) and TEM (b) images of obtained GO.

method, and the BET method was employed to determine the specific surface areas of the samples. The surface elemental composition and element valence distribution were detected by X-ray photoelectron spectroscopy (XPS) on a Kratos Axis Ultra DLD spectrometer with Al K α X-ray radiation as the X-ray source for excitation.

4. Catalytic Activity Test

The catalytic activity for the aerobic oxidation of cyclohexane was tested in a 50 mL stainless steel high-pressure reactor equipped with a magnetic stirrer. Typically, 15 g cyclohexane and 20 mg catalyst were added. Before reaction, O₂ (0.2 MPa) was injected for three times to remove the air. Then, the reactor was heated to 155 °C and the O₂ pressure of 0.8 MPa under stirring. After 90 min, the reactor was cooled to room temperature, the pressure was released and the mixture was dissolved by ethanol. The reaction products were collected and analyzed using a gas chromatograph (GC, Agilent 7820A) equipped with a flame ionization detector (FID) and an Agilent-DB-1701 capillary column. Chlorobenzene was added as internal standard. Cyclohexanone and cyclohexanol (KA oil) can be directly analyzed by GC. For the remaining cyclohexyl-hydroperoxides (CHHP), it was obtained by calculation the difference of the cyclohexanol amount before and after the addition of triphenylphosphine, which could convert the CHHP in the product into cyclohexanol. The concentration of acids and esters in the product solution was determined by chemical titration with 0.1 mol·L⁻¹ NaOH and 0.1 mol·L⁻¹ HCl.

The conversion of cyclohexane and selectivity of KA oil were calculated as follows:

$$\text{Conversion} = \frac{\text{cyclohexane consumed in molar}}{\text{initial cyclohexane in molar}} \times 100\% \quad (1)$$

$$\text{Selectivity} = \frac{\text{generated product in molar}}{\text{converted cyclohexane in molar}} \times 100\% \quad (2)$$

In the recycling catalytic experiments, the catalyst was carefully collected from the reaction mixture by centrifugation, washed thoroughly with ethanol, and dried at 80 °C overnight in a vacuum oven. Then it was subjected into the next run of oxidation reaction.

5. Computational Methods

Single-layer graphene was introduced as the support to simulate the basic structure of graphene support to carry out the theoretical calculation and investigate the influence of the nitrogen doping. All molecular modes were fully optimized by a DFT method. These modes are optimized using the dMol³ module in the Material Studio package. The exchange correlation energy of electrons was described with the Perdew-Burke-Ernzerhof (PBE) functional of the generalized gradient approximation (GGA). The calculation achieves convergence until the maximum force on each atom becomes lower than 0.004 Ha·Å⁻¹. The k-point grids of 2×2×2 were employed for structure optimization [35,36].

The binding energy of Co was calculated as follows:

$$E_{\text{bind}} = E(\text{Co+Support}) - E(\text{Co}) - E(\text{Support}) \quad (3)$$

where E(Co+Support) is the total energy of Co on the support, and E(Support) is the energy of the catalyst mode with nitrogen species or without nitrogen species. The supports investigated in

the present work include graphene, graphene with defects but without nitrogen species, and nitrogen-doped graphene (graphite N, pyridine N, and pyrrolic N) for comparison.

Finally, the length of O-O bond and deformation energy of CHHP were calculated to demonstrate the function of nitrogen doping. CHHP adsorbed on the different supports (with or without nitrogen species) loaded Co catalysts were as model.

The deformation energy of CHHP was calculated as follows:

$$E_{\text{de}} = E(\text{CHHP+Catalyst}) - E(\text{CHHP}) - E(\text{Catalyst}) \quad (4)$$

where E(CHHP+Catalyst) is the total energy of CHHP on the catalysts, and E(Catalyst) is the energy of the different supports (with or without nitrogen-doped) loaded Co catalysts.

RESULTS AND DISCUSSION

1. Catalysts Characterization Results

The textural properties of the catalysts were tested by the N₂ adsorption-desorption, and the results are shown in Fig. S1 and listed in Table 1. Fig. S1 shows that all catalysts present a IV-type isotherm associated with an H2 hysteresis loop, indicating that these samples have typical mesopores structures. The specific surface areas of the Co-N-rGO-T increased from 130.4 to 184.7 m²·g⁻¹ with increasing of the calcination temperatures from 600 to 800 °C, and it decreased again to 176.5 m²·g⁻¹ at 900 °C. That may be due to the carbon component of the material lost as the tem-

Table 1. The textural properties of the catalysts

Catalysts	BET surface area /m ² ·g ⁻¹	Pore volume /cm ³ ·g ⁻¹	Pore diameter /nm
Co-N-rGO-600	130.4	0.09	3.97
Co-N-rGO-700	179.2	0.16	4.00
Co-N-rGO-800	184.7	0.16	3.87
Co-N-rGO-900	176.5	0.22	4.22

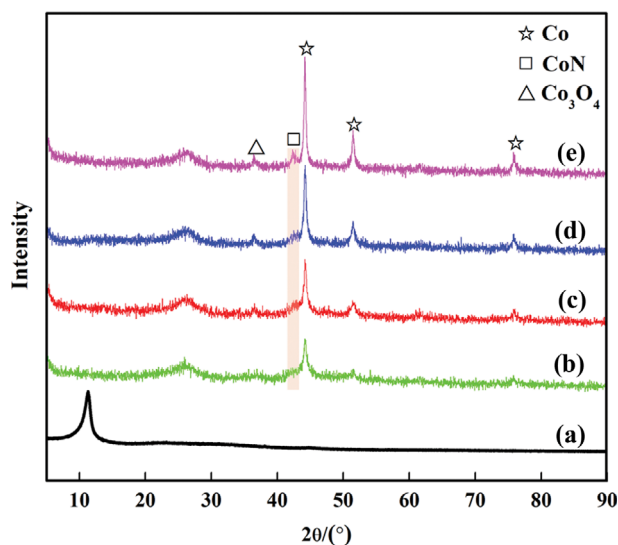


Fig. 2. XRD images of GO (a), Co-N-rGO-600 (b), Co-N-rGO-700 (c), Co-N-rGO-800 (d) and Co-N-rGO-900 (e) composites.

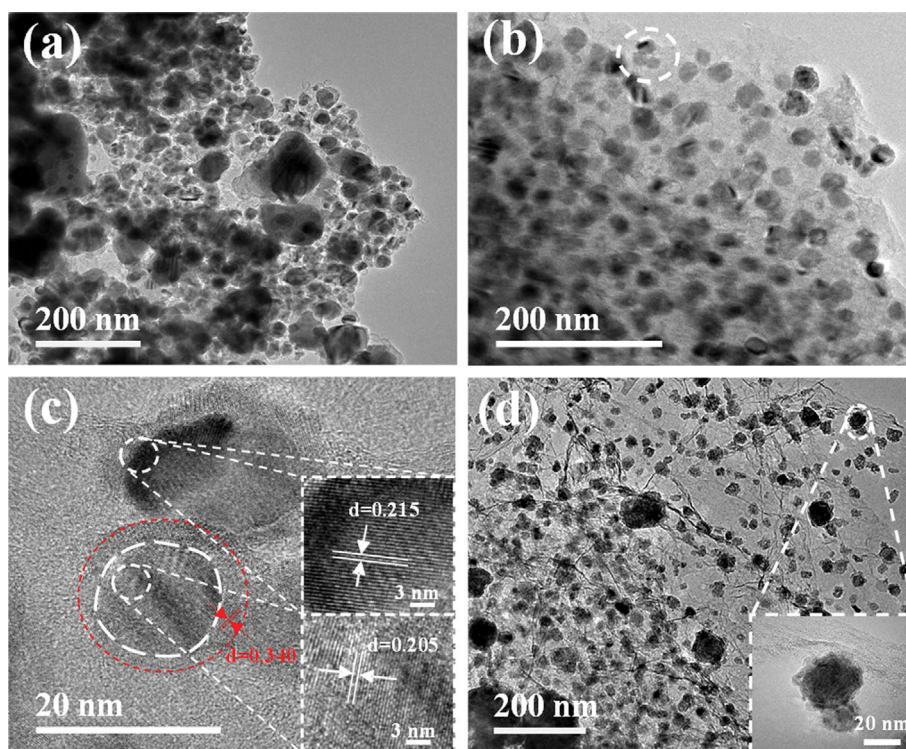


Fig. 3. TEM images of Co-N-800 (a), Co-N-rGO-800 (b), HRTEM of Co-N-rGO-800 (c), Co-rGO-800 (d).

perature further increased. In addition, the pore volume of the samples increased from $0.09 \text{ cm}^3 \cdot \text{g}^{-1}$ to $0.22 \text{ cm}^3 \cdot \text{g}^{-1}$ from 600 to 800°C , which may be due to the break of the oxygen-containing groups on the surface of GO [37].

The XRD patterns of GO and Co-N-rGO-T are shown in Fig. 2. In Fig. 2(a), the peak at $2\theta=10.92^\circ$ corresponds to the (001) facet of GO, and no characteristic peak of graphitization was observed, which confirms successful synthesis of GO. In Fig. 2(b)–(e), the diffraction peaks detected at $2\theta=26.5^\circ$ are ascribed to the lattice planes (002) of graphite carbon. And the characteristic peaks at $2\theta=44.1, 51.5$ and 75.9° correspond to (111), (200), and (220) crystallographic planes of Co metal. The results show that Co NPs on the catalysts were reduced to Co^0 by calcinating the samples in N_2 atmosphere. The intensities of the Co peaks increase with increasing of calcination temperature. Meanwhile, a weak peak at $2\theta=36.4^\circ$ was detected and consistent with the diffraction peak of the Co_3O_4 , indicating that the Co NPs were not completely reduced to Co^0 , and it may be because the oxygen-containing group in the graphene oxide oxidizes the cobalt during the decomposition process. Furthermore, a weak peak at $2\theta=42.3^\circ$ was observed and ascribed to the diffraction peak of the CoN, and its intensity gradually increased as the calcined temperature increased.

SEM and TEM were used to observe the morphology and structure of the samples. The as-prepared GO has been shown in Fig. 1. Fig. S2 shows SEM images of Co-N-rGO-T composites. Compared with GO, the surface of composites became rough after loading Co and calcination. Besides, as the calcination temperature increased, the graphene still retained layered structure and the layers were stacked, and some particles (might be Co NPs) appeared

on the surface. Fig. 3 shows TEM image comparison of Co-N-800 (without graphene), Co-N-rGO-800 and Co-rGO-800 (without N species). As in Fig. 3(a), obvious agglomeration was observed by showing different sizes of metal particles on Co-N-800, which may be due to the absence of GO in the catalyst. While for Co-N-rGO-800 (Fig. 3(b)), well-dispersed metal NPs with a size of ~ 30 nm could be observed after GO addition. Such a phenomenon implies that GO is an excellent support for promoting metal nanoparticle dispersion on the catalyst surface. As shown in Fig. 3(c), the regular lattice fringes with a spacing of 0.205 and 0.215 nm can be indexed to the (111) and (100) planes of Co^0 , respectively. It can also be observed that each Co NPs was coated by some carbon film with a thickness of about 3–5 nm. Not only can carbon-coated cobalt NPs prevent metal leaching and improve the stability of catalyst, but also effectively prevent the aggregation of metal NPs and promote electron transfer, thereby improving catalytic activity [38]. For Co-rGO-800 (without nitrogen doping) in Fig. 3(d), Co-rGO-800 has poor metal dispersion due to no nitrogen doping. As shown in the inset of Fig. 3(d), the obtained carbon films around Co are irregular and not smooth, indicating that nitrogen doping is beneficial for formation of integrated and regular carbon film around Co metal NPs.

XPS was performed to investigate the composition and chemical states of the elements on the catalysts. As shown in Fig. 4(a), the peaks fitted at ~ 780 eV and 796 eV were assigned to Co $2p_{3/2}$ and Co $2p_{1/2}$, respectively. The peaks around 780.7 and 796.1 eV were assigned to Co^{2+} , the peak at about 778.2 eV corresponded to Co^0 , and peak at 782.6 eV corresponded to Co-N. N 1s spectra in Fig. 4(b) can be deconvoluted into three peaks, which were assigned to

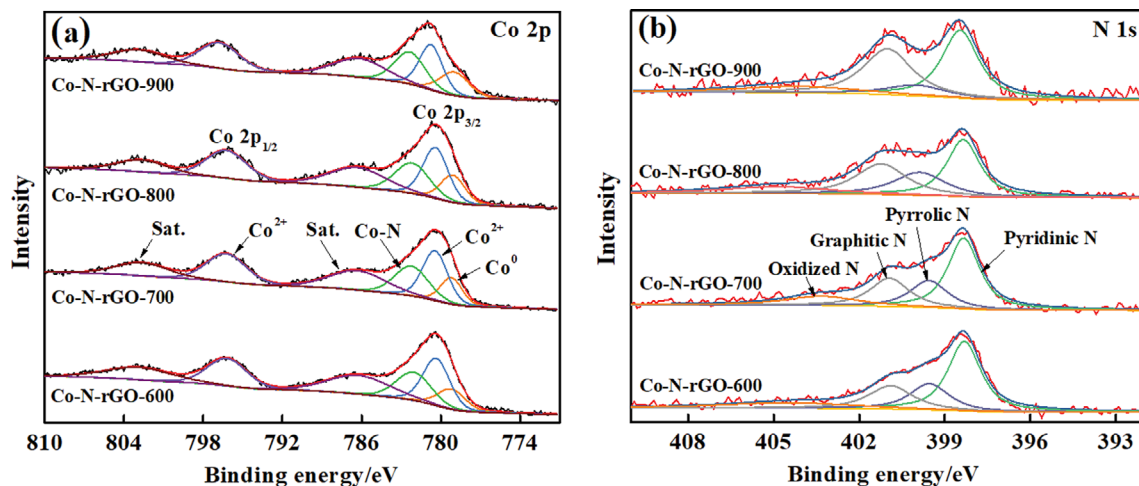


Fig. 4. XPS spectra of (a) Co 2p and (b) N 1s.

Table 2. The chemical composition of different elements over the prepared catalysts obtained by XPS analysis

Catalysts	Co /%	Different Co Con./%			N /%	Different N Con./%				O /%
		Co ⁰	Co ²⁺	Co-N		N _{pyri}	N _{pyrr}	N _{grap}	N _{oxid}	
Co-N-rGO-600	4.94	14.51	60.42	25.07	6.46	45.50	20.31	20.33	13.86	15.13
Co-N-rGO-700	3.92	14.75	59.92	25.33	5.44	44.73	20.10	21.82	13.35	11.16
Co-N-rGO-800	3.73	16.13	58.44	25.43	5.60	35.48	22.35	29.16	13.01	9.28
Co-N-rGO-900	3.22	18.46	55.29	26.25	3.22	40.63	10.42	36.44	12.51	9.15

N_{pyri}: pyridine-N, N_{pyrr}: pyrrolic-N, N_{grap}: graphitic-N, N_{oxid}: oxidized-N.

pyridinic N (~398.4 eV), pyrrolic N (~400 eV), and graphitic N (~401 eV), respectively.

Table 2 shows the chemical composition of different elements of catalysts. It shows that the concentration of Co⁰ increased with the calcination temperature, indicating that more Co NPs were reduced to Co⁰, which is consistent with XRD results. For oxygen species, its content on the surface of the material gradually decreases, and the content was much lower than that of GO (45%) [39], which shows that the oxygen-containing groups on the surface of GO continue to dissociate. For nitrogen species, the total N content decreased, and the pyrrolic nitrogen gradually transformed into pyridine nitrogen and graphite nitrogen due to its poor thermal stability as the temperature increased. Among these samples, Co-N-rGO-800 had relative high N content. In addition, Co atom in Co-N-rGO-T samples could coordinate with pyridine N to form the Co-N active sites [40–42], which may be beneficial to the improvement of catalytic performance.

2. Catalytic Performance

The catalytic performance of the prepared materials for cyclohexane oxidation reaction using O₂ as oxidant was investigated. The cyclohexane conversion was extremely low when the reaction was carried out without catalyst. Investigation of different preparation methods shows that the catalytic performance of Co-N-rGO-800 prepared by post-impregnation method was better than CoN-rGO-800 prepared by hydrothermal method and Co/NrGO-800 prepared by hydrothermal plus impregnation method under the same reaction conditions (Fig. S3). As shown in Fig. S4, CoNrGO-

800 and Co/NrGO-800 have poor metal dispersion and serious aggregation, the Co-N-rGO-800 prepared by the post-impregnation method has more uniform distribution and exposure of Co metal sites, and regular carbon film coating on Co metals that prevent it from aggregation.

By comparing Co-rGO-800 and Co-N-rGO-800 (Fig. 5(a)), rGO-800 and N-rGO-800 (Fig. 5(b)), it is notable that the content of CHHP (green bar) in the product was significantly reduced after nitrogen doping in the catalysts. Especially for Co-N-rGO-800, the content of CHHP decreased from 9.19 to 0.51 after the Co-rGO-800 catalyst was doped with nitrogen. These results show that nitrogen doping can promote the decomposition of CHHP, which is beneficial to improving selectivity to KA oil. Furthermore, the effect of calcination temperature of Co-N-rGO-T catalysts on its catalytic performance was also investigated (in Fig. 5(c)). As the calcination temperature was increased, the conversion of cyclohexane also increased. Co-N-rGO-800 shows 8.85% conversion of cyclohexane with 85.73% selectivity to KA oil. While further increasing of annealing temperature to 900 °C resulted in a lower catalytic performance, which may be due to the GO structure broken and the nitrogen content reduction at 900 °C, leading to Co-N-rGO-900 not effectively accelerating the reaction process. In addition, the catalytic performance of another popular catalyst was compared [13], as shown in Table S1. Under the same reaction conditions, the overall catalytic performance of Co-N-rGO was better than that of 0.3CeO₂-0.6NiO-Co₃O₄.

The effects of the reaction temperature, time, and O₂ pressure

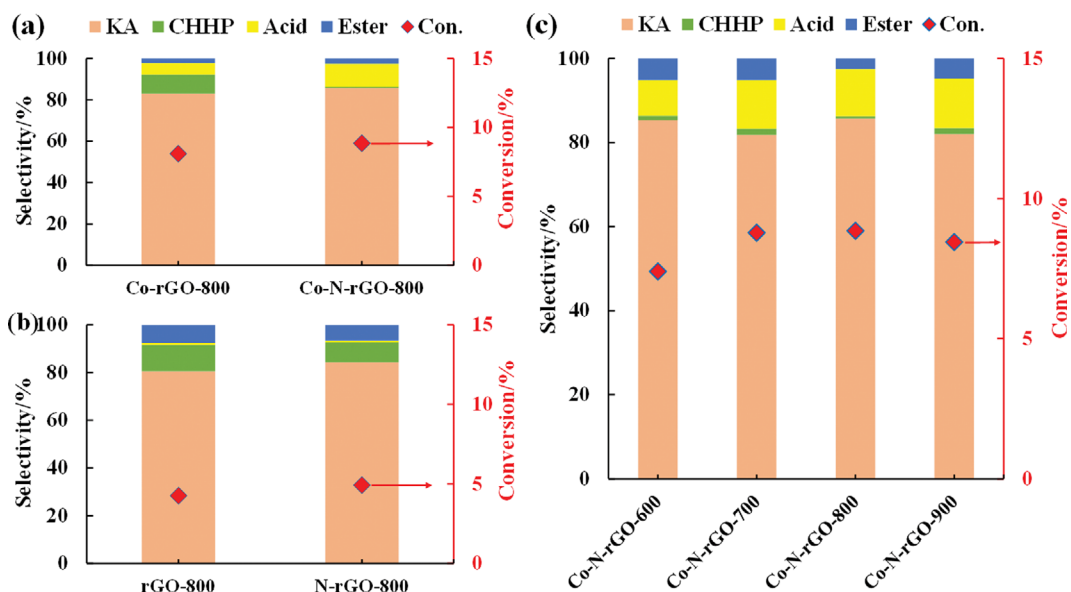


Fig. 5. The catalytic activity of the prepared catalysts in the liquid phase selective oxidation of cyclohexane. Reaction condition: cyclohexane 15 g, catalyst 20 mg, O₂ 0.8 MPa, 155 °C, 90 min.

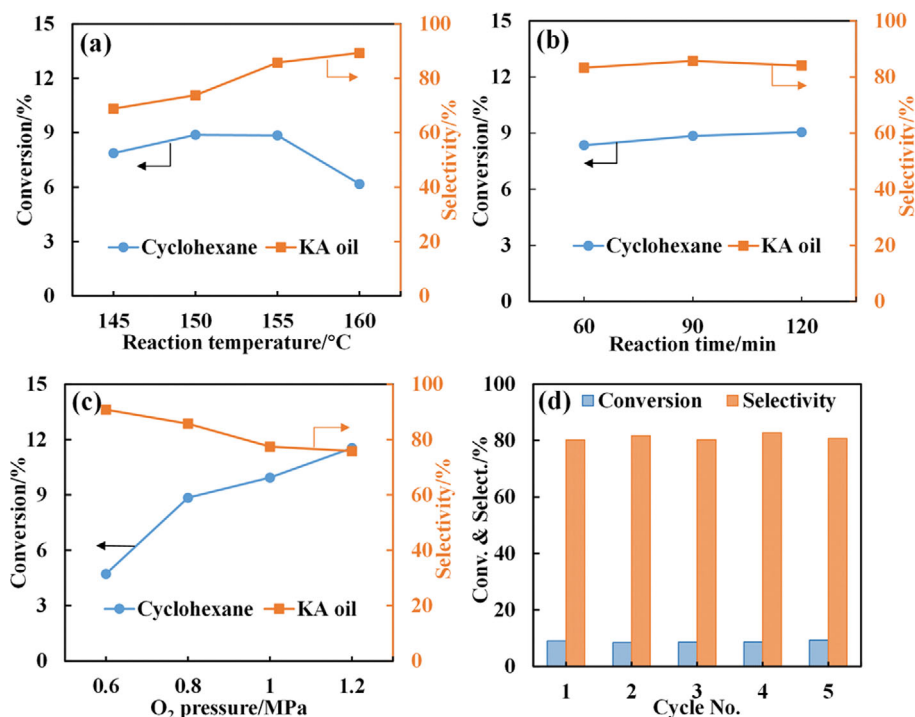


Fig. 6. Effect of the reaction temperature (a), reaction time (b), O₂ pressure (c), and the recyclability tests (d) on the catalytic activity of Co-N-rGO-800 for cyclohexane oxidation. Reaction conditions: cyclohexane 15 g, catalyst 20 mg; (a) O₂ pressure 0.8 MPa, 90 min; (b) O₂ pressure 0.8 MPa, 155 °C; (c) 155 °C, 90 min; (d) 155 °C, O₂ pressure 0.8 MPa, 90 min.

on the catalytic activity of the Co-N-rGO-800 catalyst for cyclohexane oxidation were evaluated. As shown in Fig. 6(a), the conversion of cyclohexane gradually increased from 145 to 155 °C and then decreased from 155 to 160 °C, with the KA oil selectivity increased. Taking into account both the catalytic activity and the KA oil selectivity, 155 °C was the optimized temperature. The effect of the reaction time on the activity is summarized in Fig.

6(b); the conversion of cyclohexane gradually increased as the reaction time increased, while the selectivity increased first and then slowly decreased due to the over-oxidation of KA oil, and the optimal reaction time appeared to be 90 min. Moreover, the effect of the O₂ pressure (Fig. 6(c)) shows that raising the O₂ pressure can enhance the conversion of cyclohexane, but the selectivity of KA oil decreases significantly. It demonstrated that desirable KA oil

products would be inevitably transformed into by-products under high pressure O_2 . To investigate the stability of the catalyst, recycling tests were performed over Co-N-rGO-800, and the results are shown in Fig. 6(d). There was no significant change in conversion and selectivity after five cycling reactions, and there was no obvious aggregation of metal particles on the catalyst (Fig. S5). This result confirmed that the catalyst shows very good stability.

3. DFT Calculation Results

To clarify the function of doping nitrogen species in the catalyst, a theoretical calculation was carried out based on DFT theory [35,36]. The original graphene support (without heteroatomic doping and defect), graphene support with defect but without nitrogen species, and nitrogen doped graphene support (graphite N, pyrrolic N, and pyridine N, respectively) were constructed and geometrically optimized (Fig. S6). The optimal cobalt adsorption configurations on different supports were prejudged by the comparison of three different adsorption sites of cobalt on top, bridge, and hollow. As shown in Fig. S7, the geometry optimization models were obtained by loading cobalt at the top, hollow, and bridge sites on the pyridine nitrogen site. After the geometry optimization, E_{ads} (Co/Support) (in Table 3) was calculated and the results reflect the stability of the Co atom supported on the surfaces of different catalysts. It can be seen that the adsorption energy of Co on the original graphene without heteroatoms or defects was the most unstable, while tuning the graphene support by introduction of defects and heteroatom can enhance the adsorption energy. Moreover, the adsorption of Co on the Hollow sites was more stable than that of Top and Bridge sites. Therefore, the subsequent work chooses the adsorbed cobalt in the Hollow site. The modes that underwent geometry optimization are shown in Fig. S8.

The Mulliken analysis and electron density of different models are shown in Fig. S9 and S10. To verify the effect of the nitrogen doping, the comparison of defect graphene model without nitrogen and pyridine-N graphene model is shown in Fig. 7. It can be

Table 3. The adsorption energy of Co on the different modes of modified graphene supports

Co on different support modes	Top E_{ads}/eV	Hollow E_{ads}/eV	Bridge E_{ads}/eV
Original graphene support	-1.548	-2.049	-1.619
Graphene with 12r-defect	-8.175	-8.179	-8.178
Graphene with 14r-defect	-7.564	-7.567	-7.566
Graphite-N Graphene	-1.894	-2.240	-1.764
Pyrrolic-N Graphene	-7.071	-7.071	-7.071
Pyridine-N Graphene	-1.894	-2.241	-1.901

seen that the carbon atoms near the 12r-defect exhibited much more electronic sufficient (a-1), and the electrons of the original graphene surface had not changed (Fig. S9(a-1)). After loading Co metal on 12r-defect (a-2), the carbon atoms around Co exhibited more negative charge. The above phenomena indicate that the existence of defects and cobalt loading can cause graphene electron transport on the catalysts. For Pyridine-N Graphene (b-1) and Co on the Pyridine-N Graphene (b-2), the closer carbon atoms next to nitrogen atom are more positively charged. For nitrogen itself, its charge becomes more negative after Co introduction, and the Co atom also shows more positively charged compared with (a-2) before nitrogen doping. These results indicate that there exists obvious charge transfer between nitrogen and the surrounding carbon atoms after nitrogen doping, and the nitrogen species affect the electron circumstance due to its electron pair. There also exists electron transport from Co to nearby nitrogen on the surface of the catalysts (b-2), which is beneficial to the improvement of catalytic performance.

The function of nitrogen atom doping was investigated by calculating the O-O bond length and deformation energy of CHHP on the different modes of modified graphene support loaded Co

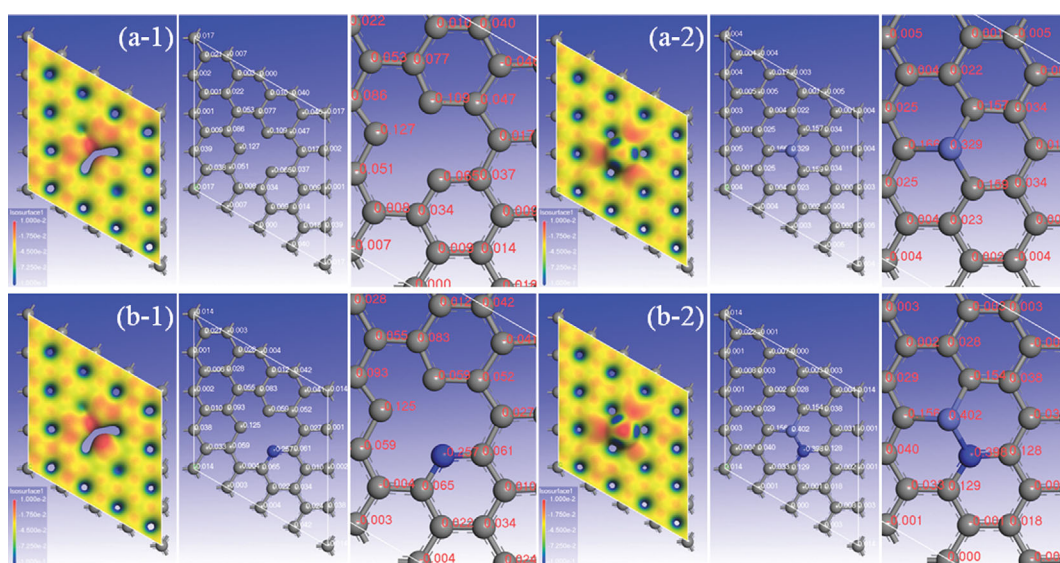


Fig. 7. The electron density and Mulliken analysis of Graphene with 12r-defect (a-1), Co on the Graphene with 12r-defect (a-2), Pyridine-N Graphene (b-1), Co on the Pyridine-N Graphene (b-2). The red color in the legend of color map represents sufficient electron whereas the blue color on behalf of the electron scarcity in electron density graphs, and the scale label is consistent.

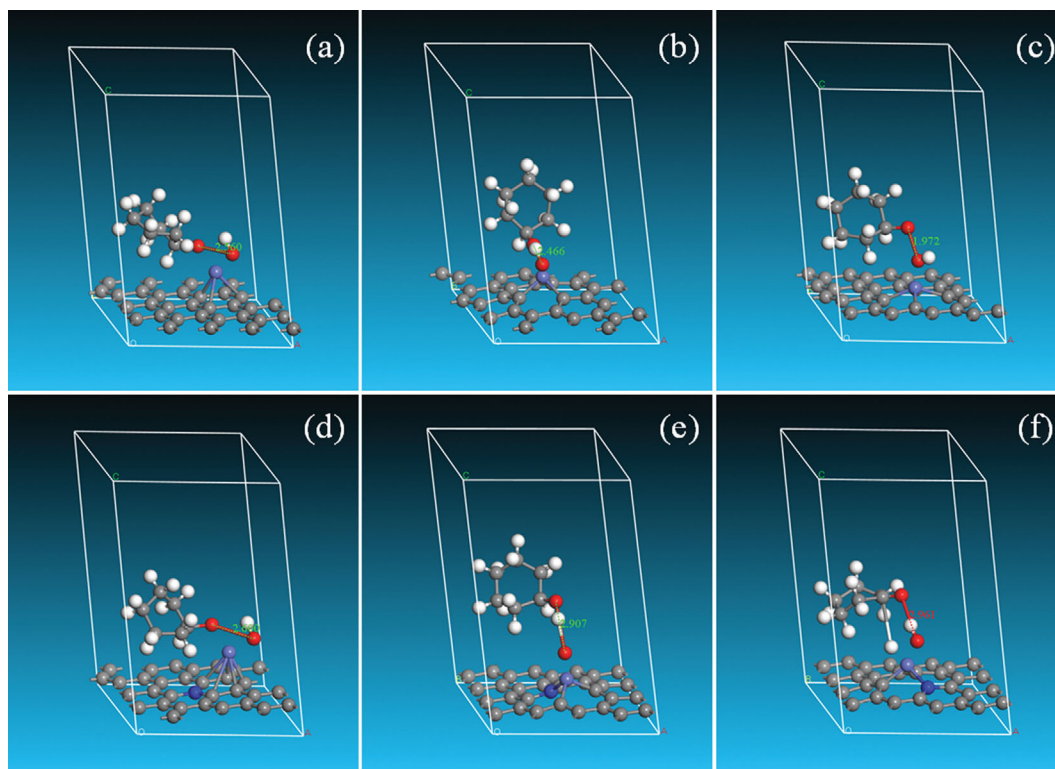


Fig. 8. The optimized CHHP adsorption configurations on Co loaded on different supports with or without nitrogen doping (parallel sites). CHHP adsorbed on graphene loaded Co (a), CHHP adsorbed on Graphene with 12r-defect loaded Co (b), CHHP adsorbed on Graphene with 14r-defect loaded Co (c), CHHP adsorbed on Graphite-N Graphene loaded Co (d), CHHP adsorbed on Pyrrolic-N Graphene loaded Co (e), CHHP adsorbed on Pyridine-N Graphene loaded Co (f).

Table 4. The O-O bond length and deformation energy of CHHP on Co loaded on the different graphene supports

Different modes	O-O bond/Å	E_{de}/eV
CHHP	1.483	-
Original graphene support	2.560	-3.887
Graphene with 12r-defect	2.466	-3.163
Graphene with 14r-defect	1.972	-3.592
Graphite-N Graphene	2.600	-3.700
Pyrrolic-N Graphene	2.907	-2.454
Pyridine-N Graphene	2.961	-2.363

with or without nitrogen doping, and the optimized modes are shown in Fig. 8. The results of O-O bond length and deformation energy on the different Co-loaded graphene materials are exhibited in Table 4. It can be seen that the O-O bond length of CHHP on the support with nitrogen doping is much larger than the one without nitrogen doping, and a lower deformation energy is observed after nitrogen doping, indicating that CHHP can be more easily dissociated on the Co load graphene support after nitrogen doping.

CONCLUSIONS

N-doped graphene loaded non-noble Co catalysts were success-

fully prepared, characterized and applied in the liquid-phase selective oxidation of cyclohexane to KA oil. The preparation method was investigated. It showed that the catalytic performance of Co-N-rGO-800 prepared by post-impregnation method was better than Co-NrGO-800 prepared by hydrothermal method and Co/NrGO-800 prepared by hydrothermal plus impregnation method. The function of nitrogen doping was also investigated; it was found that nitrogen doping is beneficial to the formation of a carbon film on the metal surface and prevents metal loss and sintering. Comparing catalytic performance of samples with or without nitrogen species shows that nitrogen doping can promote the dissociation of CHHP and enhance KA oil selectivity. DFT calculations were well consistent with the experimental observations. Moreover, effects of reaction conditions were optimized to obtain higher cyclohexane conversion and KA oil selectivity. The results show that Co-N-rGO-800 could achieve best catalytic performance of 8.85% cyclohexane conversion with 85.73% selectivity to KA oil. The catalyst could be simply recovered by centrifugation and reused for several times, and exhibit excellent stability.

ACKNOWLEDGEMENTS

This work was supported by Project of Hunan Provincial Education Department (19B572, 20B547), NSFC (21908185, 22078277), Collaborative Innovation Center of New Chemical Technologies for Environmental Benignity and Efficient Resource Utilization,

and National Department of Education Engineering Research Centre for Chemical Process Simulation and Optimization.

SUPPORTING INFORMATION

Additional information as noted in the text. This information is available via the Internet at <http://www.springer.com/chemistry/journal/11814>.

REFERENCES

- U. Schuchardt, D. Cardoso, R. Sercheli, R. Pereira, R. S. Cruz, M. C. Guerreiro, D. Mandelli, E. V. Spinacé and E. L. Pires, *Appl. Catal. A Gen.*, **211**, 1 (2001).
- A. K. Suresh, M. M. Sharma and T. Sridhar, *Ind. Eng. Chem. Res.*, **39**, 3958 (2000).
- H. Li, Y. B. She and T. Wang, *Front. Chem. Sci. Eng.*, **6**, 356 (2012).
- L. Sun, J. H. Liu, W. Luo, Y. Yang, F. Wang, C. Weerakkody and S. L. Suib, *Mol. Catal.*, **460**, 16 (2018).
- C. J. Xie, W. Wang, Y. P. Yang, L. Jiang, Y. J. Chen, J. He and J. Q. Wang, *Mol. Catal.*, **495**, 111134 (2020).
- M. Z. Wu, W. C. Zhan, Y. Guo, Y. S. Wang, Y. L. Guo, X. Q. Gong, L. Wang and G. Z. Lu, *Chinese J. Catal.*, **37**, 184 (2016).
- S. T. Wu, Y. R. He, C. H. Wang, C. M. Zhu, J. Shi, Z. Y. Chen, Y. Wan, F. Hao, W. Xiong, P. L. Liu and H. A. Luo, *ACS Appl. Mater. Inter.*, **12**, 26733 (2020).
- Z. Xiao, W. C. Zhan, Y. Guo, Y. L. Guo, X. Q. Gong, G. Z. Lu, *Chinese J. Catal.*, **37**, 273 (2016).
- X. R. Niu, Y. Y. Sun, Z. T. Lei, G. S. Qin and C. H. Yang, *Prog. Nat. Sci-Mater.*, **30**, 35 (2020).
- L. Q. Mo, X. F. Huang, G. Huang, G. P. Yuan and S. J. Wei, *ChemistryOpen*, **8**, 104 (2019).
- A. A. Alshaheri, M. I. M. Tahir, M. B. A. Rahman, T. B. S. A. Ravooof and T. A. Saleh, *Chem. Eng. J.*, **327**, 423 (2017).
- P. Zhang, J. Wang, Y. Jia, W. Q. Li, X. L. Tan, D. Zhang, S. N. Xu, P. P. Zhang, C. D. Wei and S. D. Miao, *Appl. Clay Sci.*, **181**, 105226 (2019).
- E. X. Yuan, M. Q. Gu and P. M. Jian, *Korean J. Chem. Eng.*, **37**, 1137 (2020).
- J. H. Ye, J. J. Tang, Y. J. Zhao and C. D. Wu, *Inorg. Chem.*, **59**, 767 (2020).
- P. P. Wu, Y. X. Cao, Y. Wang, W. Xing, Z. Y. Zhong, P. Bai and Z. F. Yan, *Appl. Surf. Sci.*, **457**, 580 (2018).
- C. Xu, L. L. Jin, X. Z. Wang, Y. Q. Chen and L. Y. Dai, *Carbon*, **160**, 287 (2020).
- S. Navalon, A. Dhakshinamoorthy, M. Alvaro and H. Garcia, *Chem. Rev.*, **114**, 6179 (2014).
- D. H. Long, W. Li, L. C. Ling, J. Miyawaki, I. Mochida and S. H. Yoon, *Langmuir*, **26**, 16096 (2010).
- C. N. R. Rao, A. K. Sood, K. S. Subrahmanyam and A. Govindaraj, *Angew. Chem. Int. Ed.*, **48**, 7752 (2009).
- J. L. Long, X. Q. Xie, J. Xu, Q. Gu, L. M. Chen and X. X. Wang, *ACS Catal.*, **2**, 622 (2012).
- A. K. Singh, K. C. Basavaraju, S. Sharma, S. Jang, C. P. Park and D. P. Kim, *Green Chem.*, **16**, 3024 (2014).
- G. P. Qin, X. N. Chen, L. Yang and H. M. Huang, *ACS Catal.*, **5**, 2882 (2015).
- A. Dhakshinamoorthy, A. Primo, P. Concepcion, M. Alvaro and H. Garcia, *Chem. Eur. J.*, **19**, 7547 (2013).
- X. H. Li and M. Antonietti, *Angew. Chem. Int. Ed.*, **52**, 4572 (2013).
- Z. Y. Bai, R. M. Huang, L. Niu, Q. Zhang, L. Yang and J. J. Zhang, *Catalysts*, **5**, 747 (2015).
- W. Sun, L. F. Gao, X. Feng, X. Sun and G. X. Zheng, *Eur. J. Org. Chem.*, **2018**, 1121 (2018).
- L. He, F. Weniger, H. Neumann and M. Beller, *Angew. Chem. Int. Ed.*, **55**, 12582 (2016).
- B. P. Vinayan and S. Ramaprabhu, *J. Mater. Chem. A.*, **1**, 3865 (2013).
- Y. K. Zhou, K. Neyerlin, T. S. Olson, S. Pylypenko, J. Bult, H. N. Dinh, T. Gennett, Z. Shao and R. O'Hayre, *Energy Environ. Sci.*, **3**, 1437 (2010).
- C. Wang, P. Zhai, Z. C. Zhang, Y. Zhou, J. K. Zhang, H. Zhang, Z. J. Shi, R. P. S. Han, F. Q. Huang and D. Ma, *J. Catal.*, **334**, 42 (2016).
- R. N. Shi, J. X. Zhao, S. S. Liu, W. Sun, H. X. Li, P. P. Hao, Z. Li and J. Ren, *Carbon*, **130**, 185 (2018).
- M. Favaro, S. Agnoli, L. Perini, C. Durante, A. Gennaro and G. Granozzi, *Phys. Chem. Chem. Phys.*, **15**, 2923 (2013).
- W. S. Hummers Jr and R. E. Offeman, *J. Am. Chem. Soc.*, **80**, 1339 (1958).
- Y. H. Tian, L. Xu, J. Bao, J. C. Qian, H. N. Su, H. M. Li, H. D. Gu, C. Yan and H. N. Li, *J. Energy Chem.*, **33**, 59 (2019).
- J. R. Li, R. G. Zhang and B. J. Wang, *Appl. Surf. Sci.*, **270**, 728 (2013).
- Q. G. Jiang, Z. M. Ao, D. W. Chu and Q. Jiang, *J. Phys. Chem. C.*, **116**, 19321 (2012).
- Z. Lin, G. Waller, Y. Liu, M. Liu and C. P. Wong, *Adv. Energy Mater.*, **2**, 884 (2012).
- D. Formenti, C. Topf, K. Junge, F. Ragaini and M. Beller, *Catal. Sci. Technol.*, **6**, 4473 (2016).
- N. A. Kumar, H. Nolan, N. McEvoy, E. Rezvani, R. L. Doyle, M. E. G. Lyons and G. S. Duesberg, *J. Mater. Chem. A.*, **1**, 4431 (2013).
- H. W. Liang, S. Brüller, R. Dong, J. Zhang, X. L. Feng and K. Müllen, *Nat. Commun.*, **6**, 7992 (2015).
- F. Li, H. B. Shu, C. L. Hu, Z. Y. Shi, X. T. Liu, P. Liang and X. S. Chen, *ACS Appl. Mater. Inter.*, **7**, 27405 (2015).
- Z. L. Wang, X. F. Hao, Z. Jiang, X. P. Sun, D. Xu, J. Wang, H. X. Zhong, F. L. Meng and X. B. Zhang, *J. Am. Chem. Soc.*, **137**, 15070 (2015).